Research Article | Vol. 7, No. 11 | 1 Nov 2016 | BIOMEDICAL OPTICS EXPRESS 4569
Biomedical Optics EXPRESS

Label-free fast 3D coherent imaging reveals pancreatic islet micro-vascularization and dynamic blood flow

CORINNE BERCLAZ,[1,*] DANIEL SZLAG,[1] DAVID NGUYEN,[1] JÉRÔME EXTERMANN,[1,2] ARNO BOUWENS,[1] PAUL J. MARCHAND,[1] JULIA NILSSON,[3] ANJA SCHMIDT-CHRISTENSEN,[3] DAN HOLMBERG,[3] ANNE GRAPIN-BOTTON,[4] AND THEO LASSER[1]

[1] *Laboratoire d'Optique Biomédicale, Ecole Polytechnique Fédérale de Lausanne (EPFL),1015 Lausanne, Switzerland*
[2] *Hepia, University of Applied Science of Western Switzerland, 1202 Genève, Switzerland*
[3] *EMV Immunology, Lund University, 22100 Lund, Sweden*
[4] *Danish Stem Cell Center, 2200 Copenhagen, Denmark*
[*] *corinne.berclaz@epfl.ch*

Abstract: In diabetes, pancreatic β-cells play a key role. These cells are clustered within structures called islets of Langerhans inside the pancreas and produce insulin, which is directly secreted into the blood stream. The dense vascularization of islets of Langerhans is critical for maintaining a proper regulation of blood glucose homeostasis and is known to be affected from the early stage of diabetes. The deep localization of these islets inside the pancreas in the abdominal cavity renders their *in vivo* visualization a challenging task. A fast label-free imaging method with high spatial resolution is required to study the vascular network of islets of Langerhans. Based on these requirements, we developed a label-free and three-dimensional imaging method for observing islets of Langerhans using extended-focus Fourier domain Optical Coherence Microscopy (xfOCM). In addition to structural imaging, this system provides three-dimensional vascular network imaging and dynamic blood flow information within islets of Langerhans. We propose our method to deepen the understanding of the interconnection between diabetes and the evolution of the islet vascular network.

OCIS codes: (110.4500) Optical coherence tomography; (110.6880) Three-dimensional image acquisition; (280.2490) Flow diagnostics; (170.1420) Biology.

References and links

1. M. Brissova, M. J. Fowler, W. E. Nicholson, A. Chu, B. Hirshberg, D. M. Harlan, and A. C. Powers, "Assessment of human pancreatic islet architecture and composition by laser scanning confocal microscopy," J. Histochem. Cytochem. **53**(9), 1087–1097 (2005).
2. J. Agudo, E. Ayuso, V. Jimenez, A. Casellas, C. Mallol, A. Salavert, S. Tafuro, M. Obach, A. Ruzo, M. Moya, A. Pujol, and F. Bosch, "Vascular endothelial growth factor-mediated islet hypervascularization and inflammation contribute to progressive reduction of beta-cell mass," Diabetes **61**(11), 2851–2861 (2012).
3. Z. Medarova, D. L. Greiner, M. Ifediba, G. P. Dai, E. Bolotin, G. Castillo, A. Bogdanov, M. Kumar, and A. Moore, "Imaging the pancreatic vasculature in diabetes models," Diabetes Metab. Res. Rev. **27**(8), 767–772 (2011).
4. C. H. Dai, M. Brissova, R. B. Reinert, L. Nyman, E. H. Liu, C. Thompson, A. Shostak, M. Shiota, T. Takahashi, and A. C. Powers, "Pancreatic islet vasculature adapts to insulin resistance through dilation and not angiogenesis," Diabetes **62**(12), 4144–4153 (2013).
5. J. L. Gaglia, A. R. Guimaraes, M. Harisinghani, S. E. Turvey, R. Jackson, C. Benoist, D. Mathis, and R. Weissleder, "Noninvasive imaging of pancreatic islet inflammation in type 1a diabetes patients," J. Clin. Invest. **121**(1), 442–445 (2011).
6. C. Berclaz, A. Schmidt-Christensen, D. Szlag, J. Extermann, L. Hansen, A. Bouwens, M. Villiger, J. Goulley, F. Schuit, A. Grapin-Botton, T. Lasser, and D. Holmberg, "Longitudinal three-dimensional visualisation of autoimmune diabetes by functional optical coherence imaging," Diabetologia **59**(3), 550–559 (2016).
7. J. Almaca, J. Molina, R. A. E. Drigo, M. H. Abdulreda, W. B. Jeon, P. O. Berggren, A. Caicedo, and H. G. Nam, "Young capillary vessels rejuvenate aged pancreatic islets," Proc. Natl. Acad. Sci. U.S.A. **111**(49), 17612–17617 (2014).

#273588 http://dx.doi.org/10.1364/BOE.7.004569
Journal © 2016 Received 10 Aug 2016; revised 16 Sep 2016; accepted 3 Oct 2016; published 17 Oct 2016

Biomedical Optics EXPRESS

8. Y. El-Gohary, S. Sims-Lucas, N. Lath, S. Tulachan, P. Guo, X. Xiao, C. Welsh, J. Paredes, J. Wiersch, K. Prasadan, C. Shiota, and G. K. Gittes, "Three-dimensional analysis of the islet vasculature," Anat. Rec. **295**(9), 1473–1481 (2012).
9. Y. Y. Fu, C. H. Lu, C. W. Lin, J. H. Juang, G. Enikolopov, E. Sibley, A. S. Chiang, and S. C. Tang, "Three-dimensional optical method for integrated visualization of mouse islet microstructure and vascular network with subcellular-level resolution," J. Biomed. Opt. **15**(4), 046018 (2010).
10. J. R. Henderson and M. C. Moss. "A morphometric study of the endocrine and exocrine capillaries of the pancreas," Q. J. Exp. Physiol. Cogn. Med. Sci. **70**(3), 347–356 (1985).
11. S. Bonner-Weir and L. Orci, "New perspectives on the microvasculature of the islets of langerhans in the rat," Diabetes **31**(10), 883–889 (1982).
12. T. Murakami, T. Miyake, M. Tsubouchi, Y. Tsubouchi, A. Ohtsuka, and T. Fujita, "Blood flow patterns in the rat pancreas: A simulative demonstration by injection replication and scanning electron microscopy," Microsc. Res. Tech. **37**(5-6), 497–508 (1997).
13. L. Jansson and C. Hellerstrom, "Stimulation by glucose of the blood-flow to the pancreatic-islets of the rat," Diabetologia **25**(1), 45–50 (1983).
14. N. Lifson, C. V. Lassa, and P. K. Dixit, "Relation between blood-flow and morphology in islet organ of rat pancreas," Am. J. Physiol. **249**(1), E43–E48 (1985).
15. A. M. Svensson, C. G. Ostenson, and L. Jansson, "Age-induced changes in pancreatic islet blood flow: evidence for an impaired regulation in diabetic gk rats," Am. J. Physiol. Endocrinol. Metab. **279**(5), E1139–E1144 (2000).
16. L. Jansson, A. Barbu, B. Bodin, C. J. Drott, D. Espes, X. Gao, L. Grapensparr, O. Kallskog, J. Lau, H. Liljeback, F. Palm, M. Quach, M. Sandberg, V. Stromberg, S. Ullsten, and P. O. Carlsson, "Pancreatic islet blood flow and its measurement," Ups. J. Med. Sci. **121**(2), 81–95 (2016).
17. L. R. Nyman, K. S. Wells, W. S. Head, M. McCaughey, E. Ford, M. Brissova, D. W. Piston, and A. C. Powers, "Real-time, multidimensional in vivo imaging used to investigate blood flow in mouse pancreatic islets," J. Clin. Invest. **118**(11), 3790–3797 (2008).
18. L. R. Nyman, E. Ford, A. C. Powers, and D. W. Piston, "Glucose-dependent blood flow dynamics in murine pancreatic islets in vivo," Am. J. Physiol. Endocrinol. Metab. **298**(4), E807–E814 (2010).
19. S. Speier, D. Nyqvist, O. Cabrera, J. Yu, R. D. Molano, A. Pileggi, T. Moede, M. Kohler, J. Wilbertz, B. Leibiger, C. Ricordi, I. B. Leibiger, A. Caicedo, and P. O. Berggren. "Noninvasive in vivo imaging of pancreatic islet cell biology," Nat. Med. **14**(5), 574–578 (2008).
20. D. Nyqvist, S. Speier, R. Rodriguez-Diaz, R. D. Molano, S. Lipovsek, M. Rupnik, A. Dicker, E. Ilegems, E. Zahr-Akrawi, J. Molina, M. Lopez-Cabeza, S. Villate, M. H. Abdulreda, C. Ricordi, A. Caicedo, A. Pileggi, and P. O. Berggren, "Donor islet endothelial cells in pancreatic islet revascularization," Diabetes **60**(10), 2571–2577 (2011).
21. A. Schmidt-Christensen, L. Hansen, E. Ilegems, N. Fransen-Pettersson, U. Dahl, S. Gupta, A. Larefalk, T. D. Hannibal, A. Schulz, P. O. Berggren, and D. Holmberg, "Imaging dynamics of cd11c(+) cells and foxp3(+) cells in progressive autoimmune insulitis in the nod mouse model of type 1 diabetes," Diabetologia **56**(12), 2669–2678 (2013).
22. E. Ilegems, A. Dicker, S. Speier, A. Sharma, A. Bahow, P. K. Edlund, I. B. Leibiger, and P. O. Berggren, "Reporter islets in the eye reveal the plasticity of the endocrine pancreas," Proc. Natl. Acad. Sci. U.S.A. **110**(51), 20581–20586 (2013).
23. H. Chmelova, C. M. Cohrs, J. A. Chouinard, C. Petzold, M. Kuhn, C. G. Chen, I. Roeder, K. Kretschmer, and S. Speier, "Distinct roles of beta-cell mass and function during type 1 diabetes onset and remission," Diabetes **64**(6), 2148–2160 (2015).
24. C. Chen, H. Chmelova, C. M. Cohrs, J. A. Chouinard, S. R. Jahn, J. Stertmann, I. Uphues, and S. Speier, "Alterations in beta-cell calcium dynamics and efficacy outweigh islet mass adaptation in compensation of insulin resistance and prediabetes onset," Diabetes **65** (2016).
25. M. D. Menger, P. Vajkoczy, R. Leiderer, S. Jager, and K. Messmer, "Influence of experimental hyperglycemia on microvascular blood perfusion of pancreatic islet isografts," J. Clin. Invest. **90**(4), 1361–1369 (1992).
26. M. D. Menger, P. Vajkoczy, C. Beger, and K. Messmer, "Orientation of microvascular blood flow in pancreatic islet isografts," J. Clin. Invest. **93**(5), 2280–2285 (1994).
27. O. Sabek, M. W. Gaber, C. M. Wilson, J. A. Zawaski, D. W. Fraga, and O. Gaber, "Imaging of human islet vascularization using a dorsal window model," Transplant. Proc. **42**(6), 2112–2114 (2010).
28. M. D. Menger, S. Jaeger, P. Walter, G. Feifel, F. Hammersen, and K. Messmer, "Angiogenesis and hemodynamics of microvasculature of transplanted islets of langerhans," Diabetes **38**(Suppl 1), 199–201 (1989).
29. R. A. Leitgeb, M. Villiger, A. H. Bachmann, L. Steinmann, and T. Lasser, "Extended focus depth for fourier domain optical coherence microscopy," Opt. Lett. **31**(16), 2450–2452 (2006).
30. C. Berclaz, J. Goulley, M. Villiger, C. Pache, A. Bouwens, E. Martin-Williams, D. Van de Ville, A. C. Davison, A. Grapin-Botton, and T. Lasser, "Diabetes imaging-quantitative assessment of islets of langerhans distribution in murine pancreas using extended-focus optical coherence microscopy," Biomed. Opt. Express **3**(6), 1365–1380 (2012).
31. M. Villiger, J. Goulley, M. Friedrich, A. Grapin-Botton, P. Meda, T. Lasser, and R. A. Leitgeb, "In vivo imaging of murine endocrine islets of langerhans with extended-focus optical coherence microscopy," Diabetologia **52**(8), 1599–1607 (2009).

Biomedical Optics EXPRESS

32. C. Berclaz, C. Pache, A. Bouwens, D. Szlag, A. Lopez, L. Joosten, S. Ekim, M. Brom, M. Gotthardt, A. Grapin-Botton, and T. Lasser, "Combined optical coherence and fluorescence microscopy to assess dynamics and specificity of pancreatic beta-cell tracers," Sci. Rep. **5**, 10385 (2015).
33. V. J. Srinivasan, J. Y. Jiang, M. A. Yaseen, H. Radhakrishnan, W. C. Wu, S. Barry, A. E. Cable, and D. A. Boas, "Rapid volumetric angiography of cortical microvasculature with optical coherence tomography," Opt. Lett. **35**(1), 43–45 (2010).
34. B. J. Vakoc, R. M. Lanning, J. A. Tyrrell, T. P. Padera, L. A. Bartlett, T. Stylianopoulos, L. L. Munn, G. J. Tearney, D. Fukumura, R. K. Jain, and B. E. Bouma, "Three-dimensional microscopy of the tumor microenvironment in vivo using optical frequency domain imaging," Nat. Med. **15**(10), 1219–1251 (2009).
35. M. Szkulmowski, A. Szkulmowska, T. Bajraszewski, A. Kowalczyk, and M. Wojtkowski, "Flow velocity estimation using joint spectral and time domain optical coherence tomography," Opt. Express **16**(9), 6008–6025 (2008).
36. A. Bouwens, D. Szlag, M. Szkulmowski, T. Bolmont, M. Wojtkowski, and T. Lasser, "Quantitative lateral and axial flow imaging with optical coherence microscopy and tomography," Opt. Express **21**(15), 17711–17729 (2013).
37. A. Bouwens, T. Bolmont, D. Szlag, C. Berclaz, and T. Lasser, "Quantitative cerebral blood flow imaging with extended-focus optical coherence microscopy," Opt. Lett. **39**(1), 37–40 (2014).
38. V. J. Srinivasan, S. Sakadzic, I. Gorczynska, S. Ruvinskaya, W. C. Wu, J. G. Fujimoto, and D. A. Boas, "Quantitative cerebral blood flow with optical coherence tomography," Opt. Express **18**(3), 2477–2494 (2010).
39. E. Ilegems, P. P. Van Krieken, P. K. Edlund, A. Dicker, T. Alanentalo, M. Eriksson, S. Mandic, U. Ahlgren, and P. O. Berggren, "Light scattering as an intrinsic indicator for pancreatic islet cell mass and secretion," Sci. Rep. **5**, 10740 (2015).
40. M. Brissova, A. Shostak, M. Shiota, P. O. Wiebe, G. Poffenberger, J. Kantz, Z. Y. Chen, C. Carr, W. G. Jerome, J. Chen, H. S. Baldwin, W. Nicholson, D. M. Bader, T. Jetton, M. Gannon, and A. C. Powers, "Pancreatic islet production of vascular endothelial growth factor-a is essential for islet vascularization, revascularization, and function," Diabetes **55**(11), 2974–2985 (2006).
41. B. J. A. Janssen, T. De Celle, J. J. M. Debets, A. E. Brouns, M. F. Callahan, and T. L. Smith, "Effects of anesthetics on systemic hemodynamics in mice," Am. J. Physiol. Heart Circ. Physiol. **287**(4), H1618–H1624 (2004).
42. J. D'Hoker, N. De Leu, Y. Heremans, L. Baeyens, K. Minami, C. Ying, A. Lavens, M. Chintinne, G. Stange, J. Magenheim, A. Swisa, G. Martens, D. Pipeleers, M. van de Casteele, S. Seino, E. Keshet, Y. Dor, and H. Heimberg, "Conditional hypovascularization and hypoxia in islets do not overtly influence adult b-cell mass or function," Diabetes **62**(12), 4165–4173 (2013).
43. S. A. Villalta, J. Lang, S. Kubeck, B. Kabre, G. L. Szot, B. Calderon, C. Wasserfall, M. A. Atkinson, R. A. Brekken, N. Pullen, R. H. Arch, and J. A. Bluestone, "Inhibition of vegfr-2 reverses type 1 diabetes in nod mice by abrogating insulitis and restoring islet function," Diabetes **62**(8), 2870–2878 (2013).
44. R. B. Reinert, Q. Cai, J. Y. Hong, J. L. Plank, K. Aamodt, N. Prasad, R. Aramandla, C. H. Dai, S. E. Levy, A. Pozzi, P. A. Labosky, C. V. E. Wright, M. Brissova, and A. C. Powers, "Vascular endothelial growth factor coordinates islet innervation via vascular scaffolding," Development **141**(7), 1480–1491 (2014).
45. N. Ballian, and F. C. Brunicardi, "Islet vasculature as a regulator of endocrine pancreas function," World J. Surg. **31**(4), 705–714 (2007).

1. Introduction

The pancreas is a gland located in the abdominal cavity with two distinct functions: an exocrine function involved in digestion and an endocrine function important for glucose homeostasis. The endocrine function is assumed by highly vascularized structures called islets of Langerhans, which are scattered throughout the exocrine tissue, and release hormones into the blood vessels. In rodents, these islets of Langerhans contain a core of β-cells producing insulin surrounded by α-cells, δ-cells, PP-cells and ϵ-cells producing glucagon, somatostatin, pancreatic polypeptide and ghrelin, respectively [1]. Previous studies have shown the importance of the vascularization in pancreatic islets. For instance, it has been shown that a modification of the vascularization is associated with the early onset of both type I and II diabetes [2–5]. Using functional optical coherence imaging (FOCI), we found that there is a strong correlation between the increasing inflammation of the islets and the density of their vascular network [6]. In addition, there are indications that the glucose intolerance observed in aged mice is due to a vascular impairment rather than β-cell defect [7]. The deep localization of these islets inside the pancreas in the abdominal cavity and their heterogeneous distribution throughout this organ renders imaging their vascularization challenging. During the last decades visualization with immunohistochemistry on whole mount preparation [8,9], electron microscopy [10] and methacrylate corrosion casting [11, 12] yielded anatomical information on vascularization, but these *ex vivo* techniques have been

Biomedical Optics EXPRESS

solely restricted to structural information. Microsphere based techniques go beyond this limitation by extracting functional blood flow information in the exocrine and endocrine pancreas [13–16]. However, they require the dissection of the animal to determine the blood flow. These endpoint measurements prevent the assessment of the full blood flow dynamics and alterations in identical islets during diabetes progression. *In vivo* imaging of the vascularization of islets has been achieved through intravital fluorescence microscopy either in the native pancreas [4, 17, 18], in grafted islets in the anterior chamber of the eye [19–24] or in striated muscle by using a dorsal skin-fold window [25–28]. However, fluorescent microscopy requires both genetically modified mice expressing fluorescent proteins to detect specific cellular populations and the injection of labelled dextran or labelled red blood cells to image the vascularization and quantify blood flow. Moreover, three-dimensional islet imaging requires optical depth sectioning which implies a trade-off between axial and time resolution and prevents a complete characterization of functional parameters. Therefore, there is a need for an alternative imaging technique having a good spatial resolution, high sensitivity, sufficient penetration depth, and fast image acquisition rate to study longitudinally and non-invasively the vascularization and blood flow of islets of Langerhans. Extended-focus Optical Coherence Microscopy (xfOCM) [29] has been applied to image islets of Langerhans *in vivo* and *ex vivo* [6, 30–32]. In OCM, the axial resolution is determined by the spectral width of the broadband light source whereas the lateral resolution and depth of field are determined by the classical Abbe criteria. As a consequence increasing the numerical aperture of the objective decreases the depth of field in classical Optical Coherence Tomography systems. xfOCM overcomes this limitation by using a Bessel beam creating an elongated illumination field. These advantages enable the visualization of vascular network by motion contrast between static structures and moving red blood cells. However, the dynamics of blood flow and velocity are also important parameters to assess the functionality of the islets of Langerhans. In this paper, we demonstrated for the first time, quantitative values of pancreatic blood flow in whole islets *in situ*. Additionally, we confirm longitudinal imaging of islets over an extended period of 10 months using the graft technique in the anterior chamber of the eye (ACE).

2. Research design and methods

2.1. Animals

Prior to pancreas imaging, ICR mice were anaesthetized by an intraperitoneal injection of a 10 µl/g of body weight solution containing 9 mg/ml Ketasol and 1.45 mg/ml Xylasol. For imaging sessions longer than 30 minutes, the anaesthesia was prolonged with 1% isoflurane oxygen mixture (0.8-1 L/min). *In vivo* xfOCM pancreas imaging was performed by making a small incision of 0.5 - 1 cm through the flank of the anaesthetized mouse and by gently extracting the duodenum encircling the pancreas. A small pillar was used for stabilizing the duodenum during imaging acquisition. Both the pancreas and the duodenum were frequently humidified with 0.9% NaCl. For ACE imaging, mice (BALB/C or white B6-albino mice) were anesthetized in an induction box with 3% isoflurane mixed with oxygen (0.8-1 L/min). For imaging the anesthesia was maintained between 1-2% isoflurane. Physiological parameters (heart rate, arterial oxygen saturation and breath rate) were monitored with a pulse oximeter (MouseOx Plus, Starr Life Sciences) with a thigh sensor. Mouse head and eyeball were restrained as previously described [19].

2.2. xfOCM instrument and data recording

The xfOCM instrument is designed and built for small animal research (Fig.1). The core of this OCM set-up is a Mach-Zehnder interferometer with decoupled illumination and detection paths. A broadband infrared light source (Ti:Sa laser, Femtolasers; λ_c=800nm, $\Delta\lambda$=135nm) is split into reference and sample arm. An axicon lens in the sample arm generates a Bessel

Biomedical Optics EXPRESS

beam, which is raster scanned in the lateral dimensions to obtain tomograms with high spatial and temporal resolution. A 10x objective (a water immersion N-Achroplan 10x/0.3 or an air Neofluar 10x/0.3, Carl Zeiss objective) ensures a lateral resolution of 1.3 μm over a depth of 400 μm. After combining the sample back-scattered light field with the reference field, the resulting spectral interferogram is recorded by a customized spectrometer based on a holographic transmission grating and a high-speed line-scan camera (Basler Sprint spL4096-140km, 2048 pixels). The axial resolution, dependent on the light source bandwidth and on the spectrometer, is approximatively 3 μm in tissue. The acquisition rate was set between 5 and 70 kHz depending on the protocol used (angiography, blood velocity or blood flow) and on the tissue stability. The illumination power measured at the sample plane was around 5 mW.

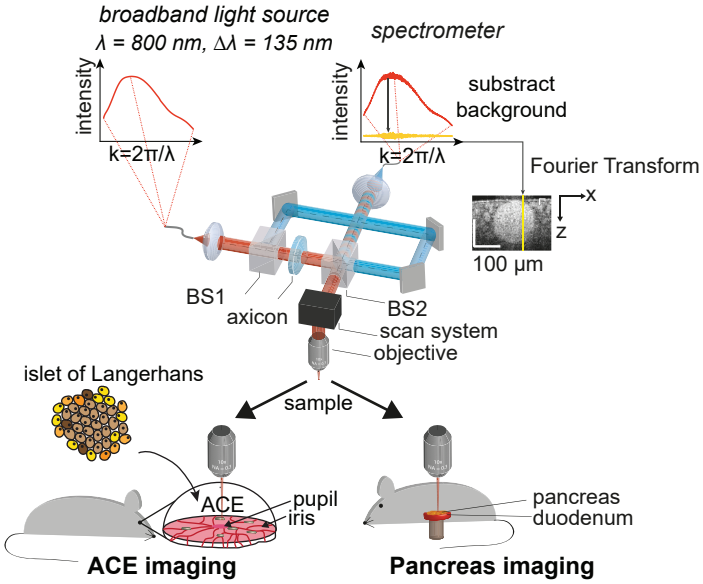

Fig. 1. xfOCM imaging setup for pancreatic islets imaging. A broadband light source is split by a beam-splitter BS1 into a sample (red) and reference (blue) arm. The back-reflected light from the sample is recombined with the reference arm by beam-splitter BS2 and detected by a spectrometer to yield the structure in depth of *in situ* islets in the pancreas or in grafted islets in the anterior chamber of the eye (ACE).

2.3. Data processing

At each lateral position the recorded spectrogram was processed to extract the tissue structure in depth. After subtracting the signal background, k-mapping followed by a Fourier transformation was applied. The depth structure is displayed by taking the logarithmic squared norm of the Fourier transform and assume an index of refraction in the pancreas close to n=1.33. Regarding the vascularization both structural and dynamic imaging can be performed (Fig. 2). Structural imaging discriminates between static tissue and moving red blood cells to reveal the vascular network, while dynamic imaging measures the Doppler frequency shift to deduce blood flow velocities. The structural imaging of moving red blood cells is obtained by modifying the standard raster scanning approach. It is based on a specific scanning protocol where each line (B-scan) is scanned several times and processed with a phase variance algorithm [33, 34] (Fig. 2(a)). This data analysis provides a specific contrast of moving scatterers such as red blood cells. For pancreas imaging, 6 to 8 B-scans were taken to perform averaging depending on the stabilization

Biomedical Optics EXPRESS

achieved, whereas for ACE imaging, 8 B-scans were averaged. Extraction of the islet and vascular volumes were done using algorithms described in previous papers [6, 30]. The vascular density is defined as the ratio between the vascular volume and the islet volume.

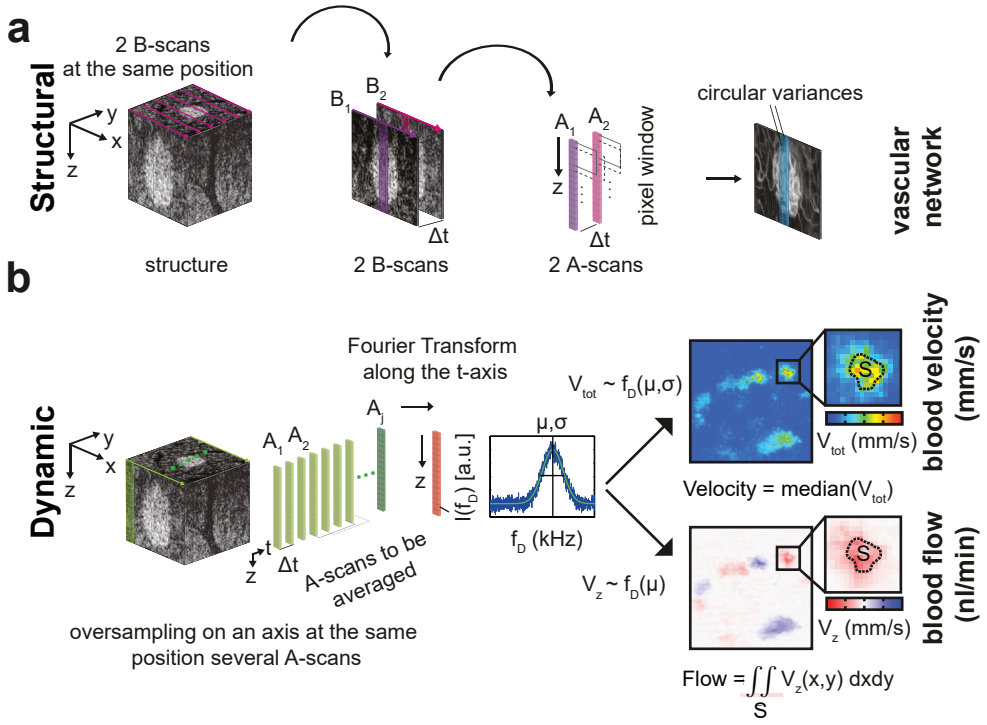

Fig. 2. Schematic representation of the data processing. **a**: Structural data processing to extract vascularization. Lateral scans are taken at the same position but with a time delay Δt and the A-scans are analyzed two by two along the time axis to extract the circular phase variance. For our measurements an axial pixel window of 8 was applied. **b**: Dynamic data processing to extract blood velocity or blood flow. μ and σ are the weighted mean and standard deviation of the Doppler spectrum, respectively. μ and σ are used to extract the total velocity V_{tot} whereas only the axial velocity component V_z is used to compute the blood flow.

We measured two dynamic parameters: (i) blood velocity and (ii) blood flow. These parameters are extracted by adapting a joint Spectral and Time domain approach (jSTD) to get the axial and transversal velocities [35, 36]. C-scans of 128x4096x1024 pixels were acquired by scanning laterally over 200x200 μm. The data are oversampled along the lateral dimension corresponding to the fast axis of the scanning unit in order to obtain several points at the same transverse location (Fig. 2(b)). Vessels were segmented by applying thresholding and morphological operators. Blood velocity was computed using the axial and transversal velocity components to get the so-called total velocity [36, 37]. The median flow velocities over vessel cross-sections were performed to get an estimated velocity. Blood flow was computed according to the method described by Srinivasan et al. [38], where for each *en face* view in a stack, the axial velocities were integrated over each vessel cross-section to extract the flow in nl/min. This approach does not require the explicit computation of the vessel angles, which would be cumbersome to determine within the tortuous islets vascular network. The integration time was fixed to 12 μs. It allows performing sequential acquisitions of vascular network and blood flow/velocity protocols without adjusting the intensity in the reference arm. The automatic segmentation of the vessel cross-sections can

Biomedical Optics EXPRESS

result in false positive vessels. To discriminate the true vessel cross-sections from these false positive detections, we applied some criteria. In each vessel cross-section, we expect exclusively positive or negative axial velocity components. However, due to noise or aliasing of the Doppler frequency, some vessels contain both positive and negative components. We computed the ratio of negative and positive velocities and vessels with a ratio smaller than 15% were kept. For the transversal velocity component, a valid estimated velocity was defined as $\mu + 2\sigma < \frac{f_s}{2}$, where f_s is the acquisition frequency, and μ and σ are the weighted mean and standard deviation of the Doppler spectrum, respectively. Indeed, pixels satisfying this constraint have a Doppler spectrum, which is correctly sampled without aliasing. Similarly to the axial component, only vessels with at least more than 85% of valid estimated velocity were considered.

3. Results

3.1. Islet imaging inside the pancreas

We demonstrated that it is feasible to image islets of Langerhans and their vasculature *in situ* without any labeling by surgically exposing the pancreas of live animals (Fig. 3(a-c) and 4). The

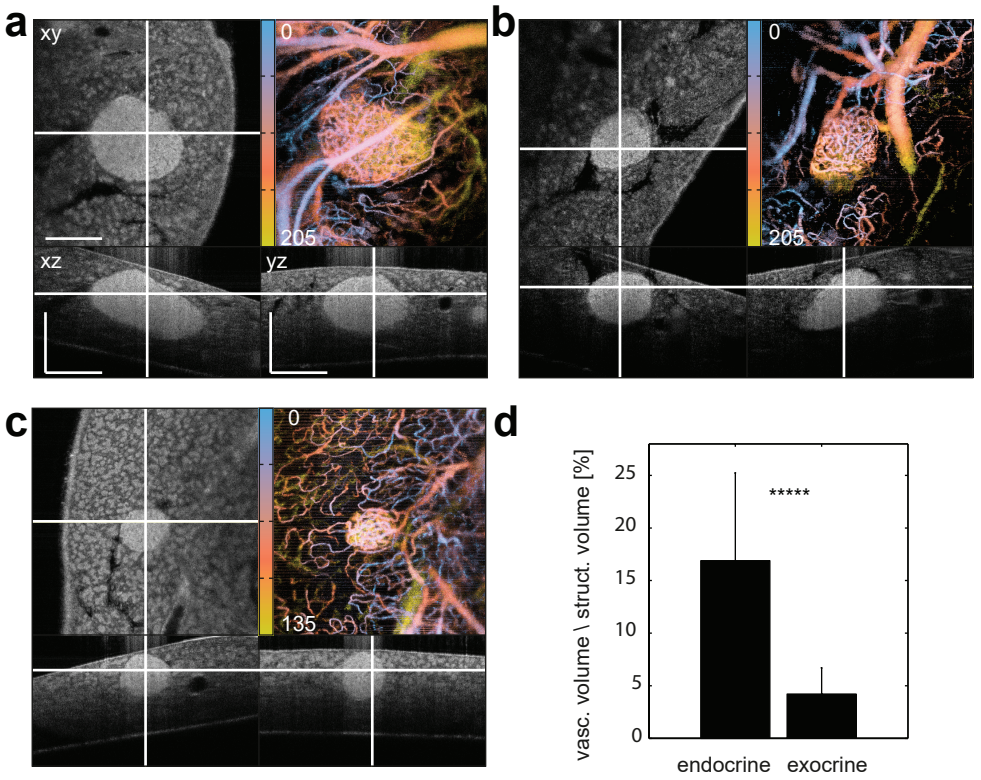

Fig. 3. Structure and vascularization of islets of Langerhans *in situ*. Representative (**a**) large islet (13.7x10^6 µm^3), (**b**) medium islet (7x10^6 µm^3) and (**c**) small islet (2.7x10^6 µm^3). **d**: Quantification of the vascular density, i.e, the vascular (vasc.) volume divided by the structural (struct.) volume in the exocrine and endocrine part. The p-value (*****) computed using a Mann-Whitney non-parametric U-test is smaller than 10^{-5}. 9 mice imaged and 16 islets analyzed. Colorbar indicates the depth in µm. Scale bar: 200 µm.

intrinsic OCM contrast for the β-cells is caused by the zinc-insulin nanocrystals [6,39], providing

Biomedical Optics EXPRESS

a strongly enhanced light scattering. Vascularization imaging can be achieved by extracting the scattering of moving red blood cells. Our imaging reveals a highly dense and tortuous vascularization inside the islets of Langerhans compared to the adjacent exocrine pancreas. We measured an endocrine vascular density of 17% agreeing with data reported from Dai et al [4]. We found the islets to be four times more vascularized than the exocrine part (Fig. 3(d)). Our result is almost twice as large as the 2.4 ratio between the endocrine and exocrine vascular density reported by Brissova et al. [40]. This difference could be explained by the variation of vascular density of the exocrine tissue as shown in Fig. 4. The acquisition time for the three-dimensional stacks shown is realized within a minute. Decreasing the scanned area and the number of averaged signal can reduce the acquisition time. Beyond the structural vascular network, OCM can be

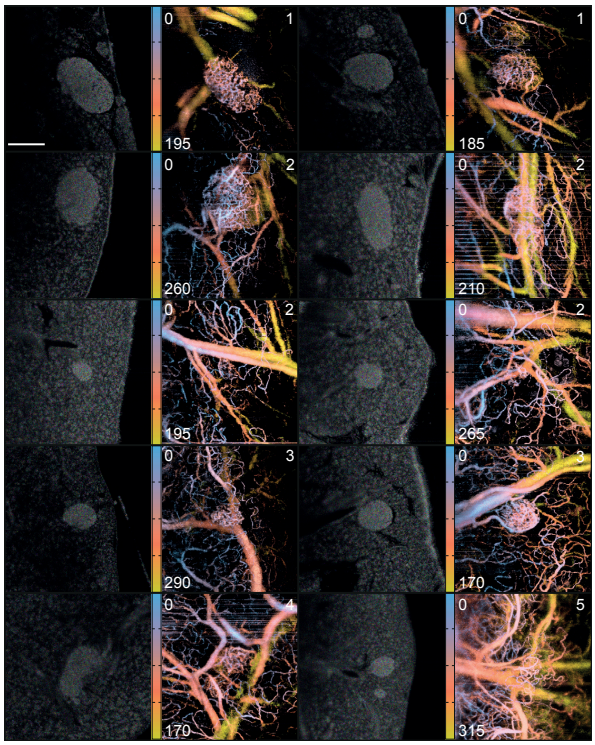

Fig. 4. Maximum depth projections of the vascular network and corresponding en face views of the tissue structure for different islets. The number in the top-right corner indicates in which mouse the islets were imaged from. Colorbars indicate the depth in μm. Stability of the samples due to heartbeat, breathing and peristaltic movements in the duodenum occasionally lead to vertical lines in the scans (arrows). Acquisition frequency was therefore adapted between 20 or 50 kHz depending on pancreas stabilization. Whenever it was possible, we chose a slower acquisition frequency to enhance the contrast in the vascular network. Scale bar: 200 μm.

used to quantify the blood velocity. Due to stabilization issue and the oversampling requirement to extract dynamic information, pancreas blood flow measurement is feasible but challenging. Indeed, except for the main vessels, blood flow in the pancreas requires a sampling frequency of 5 to 10 kHz. Figure 5 shows axial velocities computed inside the pancreas at 5 kHz. The acquisition time for this kind of images was 10 minutes, thus requiring an excellent stabilization of the pancreas. Nevertheless, when focusing on a selected vessel, the time resolution is sufficient to extract the heart beat. Figure 6 shows a large vessel in the exocrine pancreas imaged over time.

Biomedical Optics EXPRESS

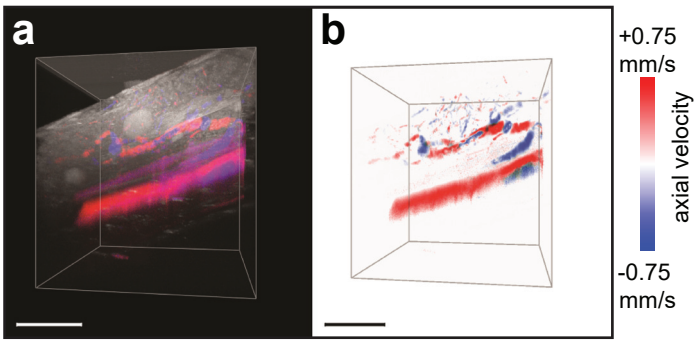

Fig. 5. Three-dimensional rendering of the axial blood velocities inside the pancreas. Red and blue color represent opposite axial blood velocity direction. **a**: Overlay of both the structural and blood flow information. **b**: Corresponding three-dimensional image showing only the axial blood velocities. Scale bar: 100 μm.

The axial component of the blood velocity along the vessel was computed and several pixels in depth were averaged to extract vessel pulsation over time (Fig. 6(c)). As presented in Figure 6(d) using a frequency analysis, the heart beat was found to be around 3.4 Hz, which is in agreement with the study of Janssen et al. in the case of mixed anesthetics [41].

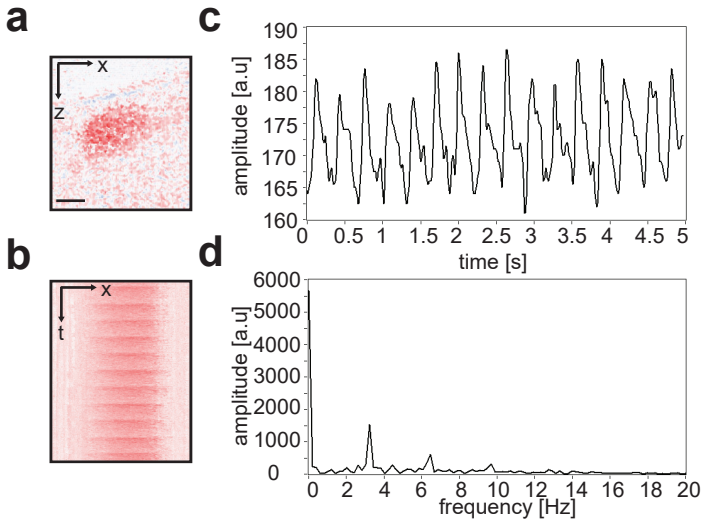

Fig. 6. Heart beat frequency. **a**: Axial components of the blood velocity inside a pancreatic vessel. **b**: Vessel pulse over time of the vessel shown in a. **c**: Pulse amplitude of the axial blood velocity over time. **d**: Frequency analysis of the signal in c. Acquisition rate was 50 kHz. Scale bar: 20 μm.

3.2. Islet imaging inside the anterior chamber of the eye

While longitudinal imaging of the pancreas is feasible, it requires heavy laparotomy and it is almost impossible to locate the same islet at successive imaging sessions. To overcome this limitation, we imaged islets grafted into the anterior chamber of the eye (ACE) of mouse, allowing to perform functional optical coherence imaging (FOCI). We showed that successive imaging of the same islets is possible over a period of 10 months (Fig. 7). This allows a quantification

Biomedical Optics EXPRESS

of the islets growth as well as the vascular density. The islets kept growing throughout the

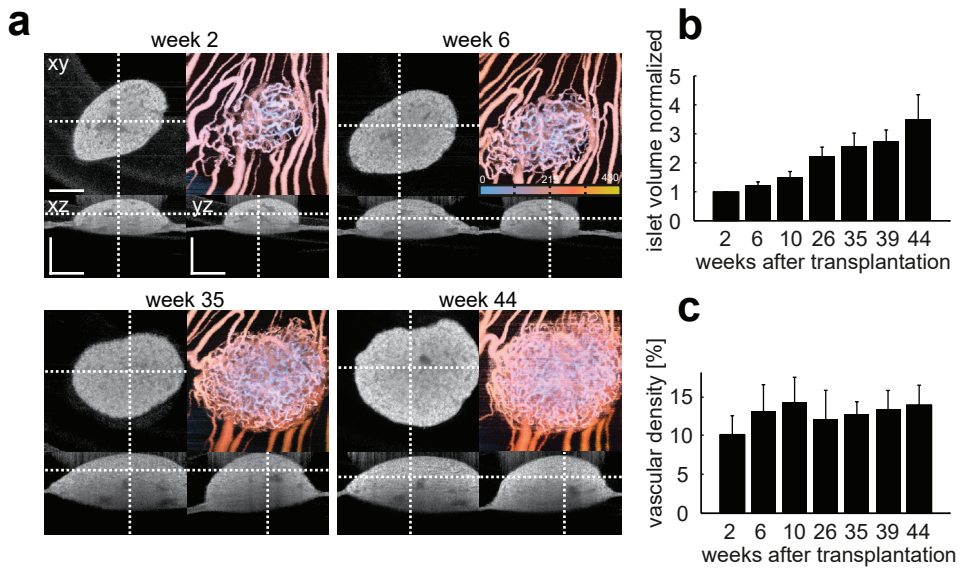

Fig. 7. Longitudinal imaging over 10 months on ACE islets. **a**: Orthogonal views of the islet structure and corresponding maximum depth projection of the vascularization at different weeks after transplantation. Colorbar indicates the depth in μm. **b**: Evolution of the volume of the islet normalized by the initial volume at week 2. **c**: Islet vascular density in percentage. Scale bar: 200 μm.

study (Fig. 7(b)), to reach a 3.5-fold increase in average volume 11 months post transplantation. Interestingly, the vascular density initially increased, but then reached a plateau at around 13% (Fig. 7(c)), which indicates an adaptation of the vascular network to the increasing islet volume. Indeed, 2 weeks after transplantation, the grafted islets have a similar vascularization as islets *in situ*. However, the ACE islet vascular density at two weeks after transplantation is still a little bit lower than the plateau reached in the following weeks (Fig. 7(c)). This percentage of vascularization is in the range of what was observed in islets *in situ* and is comparable to the vessel density measured by Almaça et al. [7] in ACE islets after an intravenous injection of fluorescent labeled dextran.

Even though ACE imaging suffers from movement artifacts (iris and eyeball movements), the stability is increased when compared to pancreas imaging. Therefore for dynamic analysis of islet blood velocities and blood flow, we focused on ACE islets. We measured blood velocities (mm/s) and blood flow (nl/min) for different vessel sizes across different islets and mice (Fig. 8). We noticed that blood flow inside the largest vessels is 19 times faster than the flow in the smallest vessels, whereas the blood velocity is only 1.2 faster. The mean blood velocity independent of vessel sizes is 1.45 mm/s. We found that the noise level for the velocity was at 0.8 mm/s and constant through the different size categories. To estimate the noise level, we computed velocities and flow in circular areas in vessel-free regions of the islets. The area size was matching the vessel cross-section size, i.e. 5.5, 12 and 25 μm diameter for small, medium and large categories respectively. The main contribution for this noise level is coming from the transversal blood velocity component whereas the noise level from the axial velocity component is only 0.01 mm/s. For the blood flow, we found a noise of 0.01, 0.04 and 0.14 nl/min, for small, medium and large blobs, respectively. This noise level represents a bias and a limit to the smallest detectable blood flow and blood velocity. The blood velocity measured with OCM values is in the range but

Biomedical Optics EXPRESS

higher than the blood velocities obtained with fluorescence microscopy by tracking individual fluorescent red blood cell in islets in the pancreas of mice [18] or fluorescent label dextran in islets grafted into a hamster dorsal skinfold preparation [25, 28]. Using intravital microscopy and combining the vessel diameter to the blood velocity, a capillary blood perfusion of 1.8 nl/min was described in islets grafted in a hamster dorsal skinfold preparation [25]. xfOCM blood flow for similar vessel diameters is 0.5 nl/min. At this stage, it is difficult to know whether these differences are due to physiological or instrumental origins, i.e, the imaging method, the specie or the islet graft site.

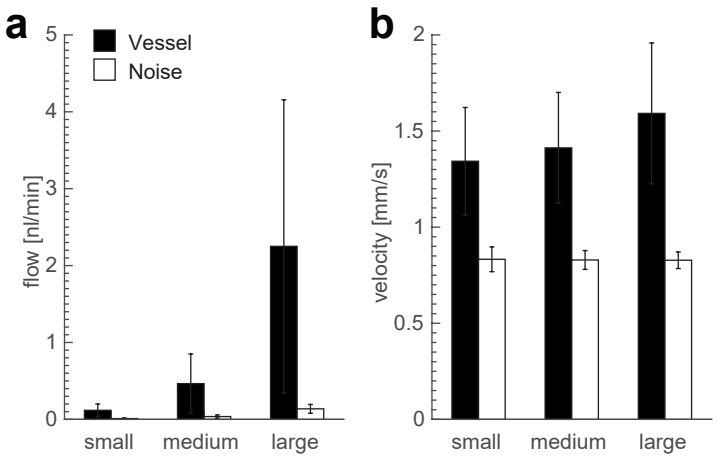

Fig. 8. Blood flow and velocities in ACE islets. **a**: Blood flow for different vessel size categories. **b**: Total blood velocity for different vessel size categories, computed from axial and transversal velocity components. Small (3-8 μm), medium (8-16 μm) and large (>16 μm) vessel diameter sizes. Acquisition frequency: 10 kHz. 3 mice were imaged. Small: 1218 cross-sections analyzed, medium: 1441 cross-sections analyzed, large: 465 cross-sections analyzed. The diameter of the vessels were determined using the minor axis length returned by the function *regionprops* from Mathworks, which returns properties for each connected components in an image. The noise was computed in circular areas of matching size in vessel-free regions inside the islets. The p-value computed using a Mann-Whitney non-parametric U-test is smaller than 10^{-5} for all groups.

4. Conclusion

We have established a label-free imaging technique with spatial micrometric resolution, a high sensitivity to detect individual islets with their vascularization and monitor blood flow properties *in situ* and in the ACE graft site. *In vivo* xfOCM depth penetration is limited to approximatively 500 μm, therefore for large islets only a part can be imaged. In particular, vascularization imaging presents shadowing artifacts, resulting in an artificially extended signal of the vasculature in depth. Compared to fluorescent intravital microscopy, OCM label-free imaging of vascularization eliminates bleaching or toxicity of the fluorescent contrast agent, rendering OCM suitable for longitudinal studies in live animals. In addition, xfOCM is contact free and does not require a coverslip or to detach the spleen to image the pancreas. Sor far, studies on islet vascular density have mainly be performed *ex vivo* by staining markers of endothelial cells [40, 42–44]. Intravital microscopy has been used to reveal the vascular network in islet [4, 17, 45] and to extract blood velocity [17, 25, 28]. However, these methods only focus on subpart of vessels lying in a defined

Biomedical Optics EXPRESS

axial plane whereas OCM can simultaneously resolve all the pixels along the axial dimension, thereby analyzing several vessels in parallel. This multiplexing advantage allows resolving blood velocity and flow dynamic as well as to analyze several vessels including a full volume. Acquisition time with xfOCM varies according to the information to extract: a field of view of 800 μm^2 requires between 5 to 15 seconds for structure and at least twice this time to extract the structural vascular network. Acquisition of resolved blood velocity over 400 μm (B-scan) requires between 1-2 seconds, and for a small volume (C-scan) scanned over 200x200 μm blood flow and velocity can be measured in 30 seconds to 1.7 minutes depending on the acquisition frequency.

In conclusion, fast xfOCM imaging combined with the longitudinal feature of the ACE model (FOCI) opens the door to study the interaction between islets of Langerhans, its vascular network and blood flow under physiological and pathological conditions and to monitor during several weeks the effects of anti-diabetic drugs on individual islets with micrometric resolution.

Funding

European Commission within the 7th Framework Programme (EU FP7-222980); Scientific Exchange Programme between Switzerland and the New Member States of the European Union (Project Code: 10.228).

Acknowledgments

We thank Vincent Shamaei (EPFL) for his help with the development of user interfaces for image processing. C.B and D.S contributed equally to this work.